Investigation of beam loss mechanism by parasitic H^- in high-power proton linac

Duanyang Jia,[1,2,3] Zhijun Wang,[1,2,3,*] Huan Jia,[1,2,3] Bingyan Liu,[1,3] Man Yi,[1,3] Dalong Guo,[1,2] Hanjie Cai,[1,2,3] Weilong Chen,[1,2,3] Shuhui Liu,[1,2,3] Tielong Wang,[1,2,3] Tao Zhang,[1,2,3] and Yuan He[1,2,3,†]

[1]*Institute of Modern Physics, Chinese Academy of Sciences, Lanzhou 73000, China*
[2]*University of Chinese Academy of Sciences, Beijing 100049, China*
[3]*Advanced Energy Science and Technology Guangdong Laboratory, Huizhou 516001, China*

(Received 25 January 2025; accepted 6 August 2025; published 10 September 2025)

Beam loss is the most critical topic in the high-power accelerator community. During high-power proton beam commissioning of Chinese ADS Front end, unexpected irradiation dose was detected opposite to the proton beam deflection direction. This indicates that there are parasitic H^- particles inside the proton beam, which were first observed in the linac facility. In the paper, regarding this beam loss phenomenon, a qualitative analysis was carried out through nuclide analysis and was based on the theoretical foundation of molecular science. Moreover, a quantitative analysis was conducted through beam experiments, and finally verified this beam loss mechanism, which needs to be considered in the future design of high-intensity and high-power proton accelerators.

DOI: 10.1103/4tgj-mxmv

I. INTRODUCTION

Beam loss is a key issue in high-power accelerators, which is the direct limitation for the high-power operation. For hands-on maintenance purposes, it is necessary to maintain the beam loss below 1 W/m for superconducting (SC) proton and heavy ion linacs [1]. Common beam loss mechanisms in linacs include beam halo formation, dark current from the ion source, or rf turn on/off transients [2]. In general, most injectors of accelerator facilities choose to accelerate H^- beam due to the requirement for injection into storage rings. This is because charge-exchange injection can overcome the constraints imposed by Liouville's theorem. However, compared to proton accelerators, H^- accelerators have more beam loss mechanisms and are more difficult to control beam loss [3]. During the operation of J-PARC linac, beam loss caused by residual gas stripping was observed in the whole section [4]. The electrons are stripped off the H^- particles by the residual gas (H_2, H_2O, CO_2, etc.), leaving behind a hydrogen atom or a proton. Another beam loss mechanism is H^+ capture and acceleration. Two electrons are stripped due to interactions between the H^- beam and residual gas, thereby generating protons, and it will be captured by the rf buckets, accelerated along with the main beam, and ultimately lost in the HEBT section [5]. This mechanism has been observed in both J-PARC and LANSCE [6]. Recently, SNS has discovered a new type of beam loss mechanism called intrabeam stripping [7], in which the interaction between H^- particles causes electrons to be stripped away, leaving neutral H^0 particles that are subsequently lost due to lack of focusing.

These beam loss mechanisms are all caused by the interactions within the beam or between the H^- beam and residual gas, but there are no similar beam loss mechanisms reported for proton accelerators yet.

In the paper, a beam loss mechanism was observed and verified in the proton accelerator, qualitative and quantitative analyses were conducted on this mechanism based on theoretical studies and experimental measurements.

II. UNEXPECTED BEAM LOSS DETECTION AT CAFE

In order to validate the viability of the accelerator driven subcritical system (ADS) [1], a demo facility was constructed to demonstrate the technical practicability of the high-power SC linac. Chinese ADS Front end (CAFe) consists of an electron cyclotron resonance (ECR) ion source with 2.45 GHz frequency, a low-energy beam transport line (LEBT), a radio frequency quadrupole (RFQ), a medium energy beam transport line (MEBT), an SC section, a high-energy beam transport line (HEBT), and a high-power beam dump [8]. The frequency of both

*Contact author: wangzj@impcas.ac.cn
†Contact author: hey@impcas.ac.cn

Published by the American Physical Society under the terms of the Creative Commons Attribution 4.0 International license. Further distribution of this work must maintain attribution to the author(s) and the published article's title, journal citation, and DOI.

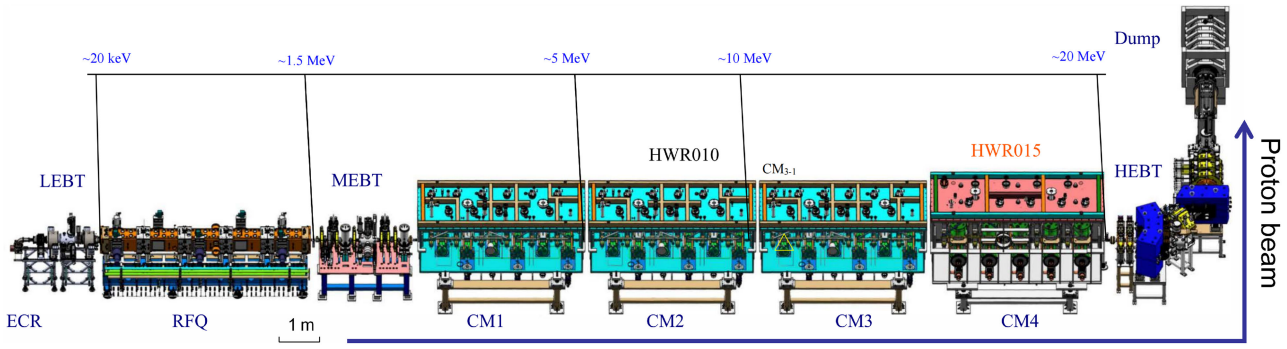


FIG. 1. Layout of CAFe.

the RFQ and the SC section cavity is 162.5 MHz. The layout of CAFe is shown in Fig. 1. The beam parameters of the CAFe are shown in Table I.

At the beginning of 2021, CAFe began system integration and high-power operation plan. The goal was for the accelerator to operate in cw mode for more than 100 h with the beam power exceeding 100 kW (> 17 MeV, > 5 mA). Another goal was for the accelerator to operate in cw mode for more than 12 h with a beam current greater than 10 mA. After approximately 50 days of beam commissioning, CAFe achieved a highly successful high-power commissioning campaign that demonstrated long-term operation of a continuous wave (cw) beam at 10 mA.

Beam dynamics and error analysis of CAFe were carried out with Tracewin code [8]. Simulation results indicate that during the design process, the dose along the accelerator remains below the level that can be manually maintained, and even when some errors are applied, the linac can transport and accelerate the beam without any extra losses, ensuring the stability of the accelerator.

Five days after beam commissioning, the residual radiation dose inside the tunnel was measured using a handheld model 451P ion chamber survey meter. The dose along the beam transport line from the ion source to the SC section was lower than 20 μSv/h. Unexpected dose of 22 mSv/h was observed at the gate valve of HEBT right deflection position, which was opposite to the proton beam deflection direction. As for other locations at the HEBT section, the dose rate was less than 0.5 mSv/h. Due to the fact that the probe of the meter cannot approach the beam pipeline and for radiation safety reasons, there is a distance of approximately 1 m between the hot spot and the actual measurement point. Sixteen days later, a long-pole γ dose monitor was employed to measure the dose as close to the pipeline as possible. This time, the valve remained the section with the highest dose (42 mSv/h). The dose of the surrounding environment was 100 μSv/h. The measured dose distribution and measuring equipment used are shown in Fig. 2. PB in the figure denotes the background dose. The detection of the abnormal dose provided conclusive evidence that severe beam loss occurred at the right deflection gate valve.

TABLE I. Beam parameters of CAFe.

Particle	H^+	
LEBT section energy	20	keV
RFQ output energy	1.5	MeV
SC output energy	20	MeV
Beam current	10	mA
rf frequency	162.5	MHz
Operation mode	cw/pulse	

III. QUALITATIVE ANALYSIS

The beam loss issue described above led to a relatively high dose in the HEBT section. This not only posed a significant impact on the daily maintenance of the accelerator but also had an impact on the lifespan of other elements in accelerator. In this section, to pinpoint the causes of beam loss, we utilize nuclide analysis and historical operation records to determine the types of particles accountable for the beam loss as well as their generation locations.

A. Nuclide analysis

Three months following the shutdown of the CAFe, the gate valve in the hot-spot area was removed. An ultrapoly clean wiper was employed to wipe the surface of the gate valve, and the wiped sample was preserved. The nuclides on the surface of the wiped sample were measured by utilizing a low-background, high-purity germanium spectrometer (HPG) [9]. The result is shown in the Fig. 3. ^{54}Mn, ^{51}Cr, and ^{56}Co were detected in the sample, but not ^{60}Co and ^{58}Co. The result shows that most of the above-mentioned nuclides are produced by reaction between stainless steel and hydrogen, instead of neutron activation.

Possible ion species extracted from an ECR proton source include proton, H_2^+, H_3^+, and H^-. Due to the relatively weak focusing, a majority of the H_2^+ and H_3^+ particles are lost in the LEBT section, and the residual part is lost in the RFQ. Consequently, it can be ascertained that

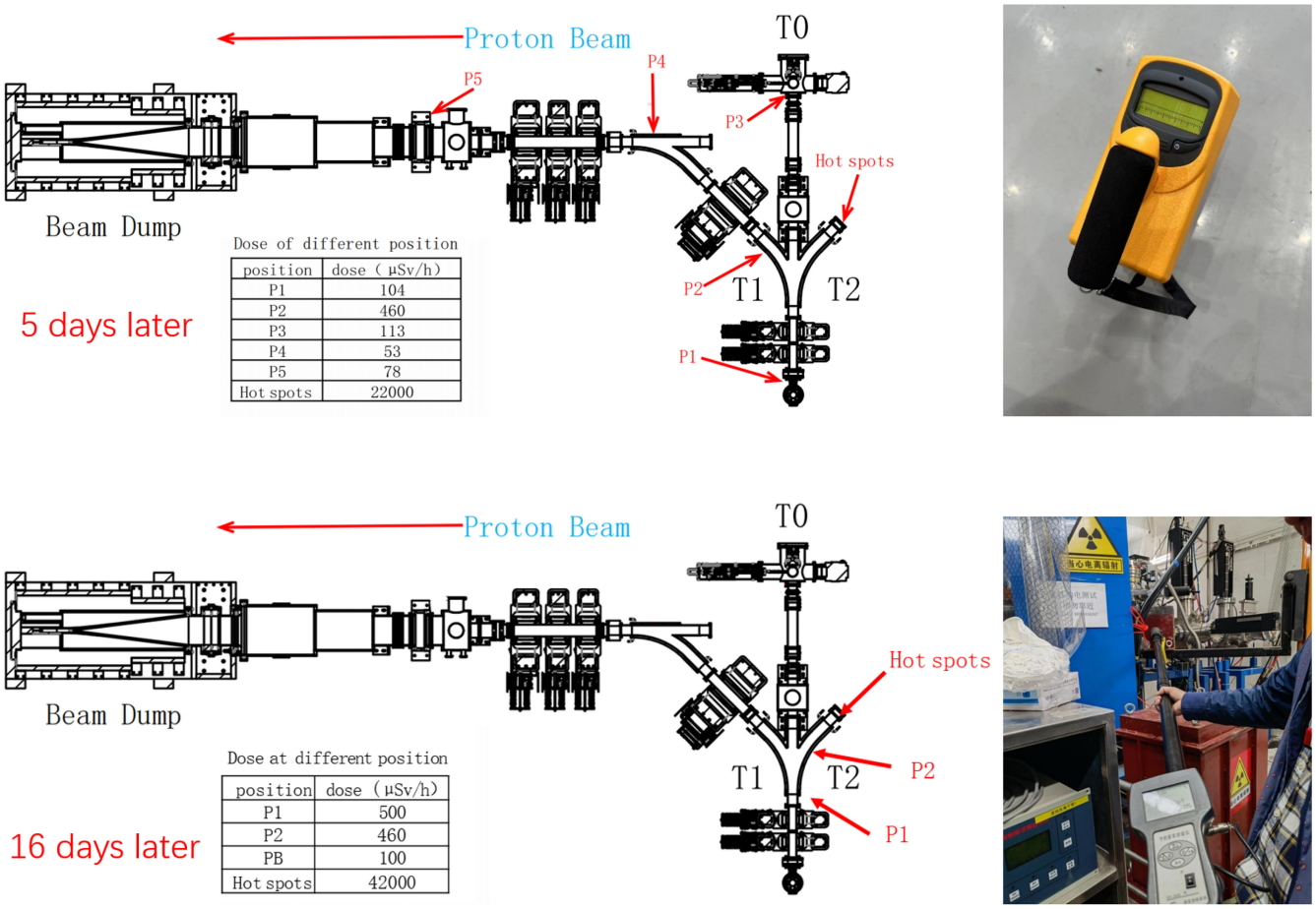


FIG. 2. Measured residual dose distribution of CAFe.

the unexpected dose was caused by the bombardment of stainless steel by either protons or H^- particles.

B. Operation record

Since the beam power of the main proton beam was greater than 100 kW, if the beam loss was caused by the main beam bombarding the valve, the valve would have been punctured very rapidly. Therefore, we can deduce that the beam loss was caused by the secondary beam.

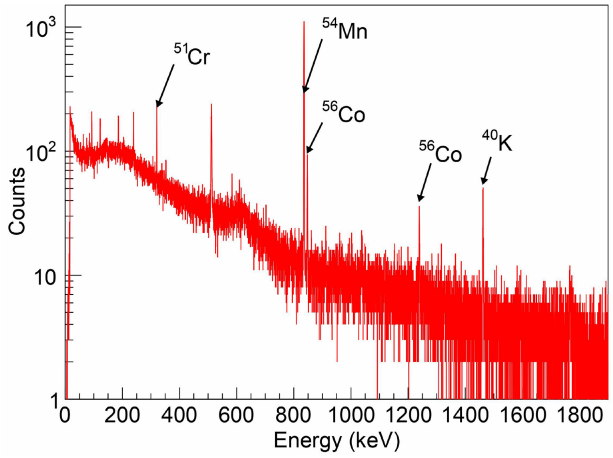


FIG. 3. Nuclide measurement results using HPG.

In order to further confirm the type of particles bombarding the stainless steel, we examined the historical records during the operation. The operation records of the power supply of the dipole magnet were surveyed and there were only positive current settings during operation. This implies that the protons in the HEBT section were deflected by the dipole magnet and then transmitted to the beam dump. Therefore, we deduced that the beam loss was caused by parasitic H^- particles.

Next, it is necessary to further confirm where the parasitic H^- particles were generated. According to the operation records, the high voltage applied to the extraction electrode of ion source was always positive during commissioning, which means that only proton beam could be extracted from the ion source. On the other hand, the reactions from protons to H^- particles mostly occur in the low-energy range, and as the energy increases, the reaction cross section rapidly decreases.

In summary, the following conclusions can be drawn. We deduced that the abnormal dose resulted from the reaction between parasitic H^- particles and stainless steel, and H^- particles were generated in the LEBT section.

IV. ACCELERATION AND TRANSPORT OF PARASITIC H^- PARTICLES

Due to the continuous generation of parasitic H^- ions along the LEBT section, the distribution of H^- ions cannot be accurately determined. Therefore, in the simulation, we assumed that at the RFQ entrance, H^- ions had the same distribution as the proton beam. The phase space distribution at the RFQ entrance is shown in Fig. 4. We simulated the dynamic processes of protons and negative H^- ions simultaneously injected into the RFQ in the CAFe accelerator using the AVAS software [10]. Figure 5 shows the longitudinal phase space distribution of proton and H^- bunches at different positions within the RFQ, where protons and H^- ions are colored in red and blue, respectively. In the radial-matching section and the early stage of the shaper section of the RFQ, the beams are injected and mixed together in dc mode. In the shaper section, the proton and H^- bunches begin to gradually separate and bunch into their respective buckets, with adjacent proton and H^- bunches having a phase difference of 180°. In the gentle-buncher section, the proton and H^- bunches continue to bunch at their respective synchronous phases, and finally accelerate to the set energies.

In addition, simulation results demonstrate that approximately 3% of H^- particles and 0.4% of protons are lost within the RFQ. The materials currently employed in RFQ exhibit surface blistering under hydrogen ion beam irradiation, which induces performance degradation and shortens service life. Therefore, the exploration of novel materials to replace traditional copper-based materials is imperative [11]. Figure 6 shows the beam envelope and phase along the machine of the MEBT and SC section. It can be seen from the simulation result that in the MEBT, the beam envelope will change significantly due to the opposite focusing forces of quadrupole magnets. At the entrance of the superconducting section, the H^- particles are not perfectly matched, resulting in a large envelope oscillation when the beam passes through the SC solenoid. However,

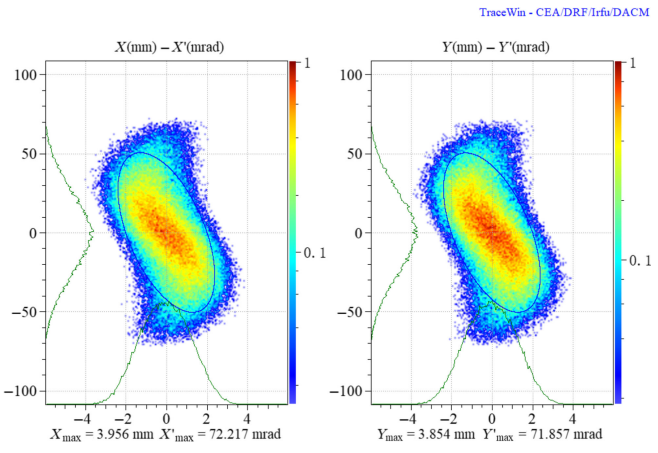


FIG. 4. Phase space distribution at the RFQ entrance.

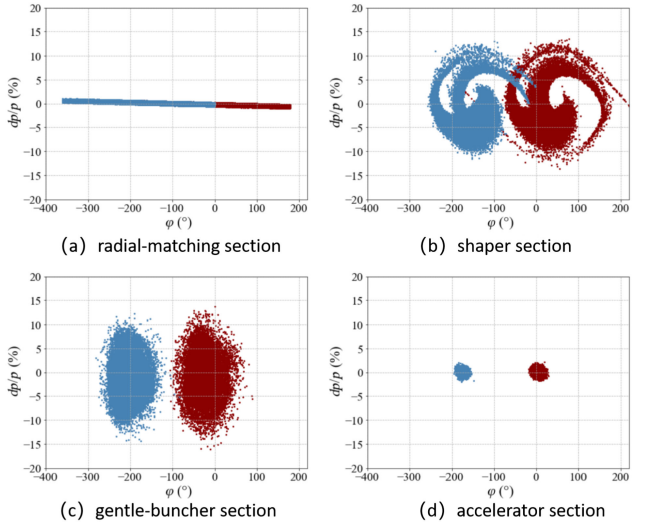


FIG. 5. Longitudinal phase space when protons and H^- ions are accelerated simultaneously in RFQ.

according to the simulation results, no H^- particle is lost along the accelerator. Ultimately, H^- particles were deflected to the right by the dipole magnet in the HEBT and hit the valve. In conclusion, the parasitic H^- particles can be transported and accelerated along with the main beam.

In the previous chapter, we have demonstrated that the beam loss mechanism results from the existence of parasitic H^- particles. In this section, we will carry out a quantitative analysis of the mechanism's yield based on molecular physics and experiments.

A. Molecular physics

We conjectured that H^- particles were mainly generated by the electron capture reaction between the proton beam and the background gas (H_2). From a molecular perspective, considering the vacuum pressure of the LEBT section, H^- particles are mainly generated via two types of reactions. One type is due to the two-electron capture reaction between protons and hydrogen gas, where a proton captures two electrons and becomes an H^- particle. The other type is due to two single-electron capture effects between protons and hydrogen gas. First, a proton captures an electron to become an H^0 particle, and then it captures another electron to become an H^- particle. It is necessary to calculate and compare to indicate which type dominates.

In the LEBT section of the accelerator with a length of L, the reaction ratio η can be expressed as [12]

$$\eta = p\frac{L}{k_b T}\sigma_{cx}, \tag{1}$$

where p denotes the background gas pressure in Pa, k_b denotes the Boltzmann constant in J/K, and T denotes the

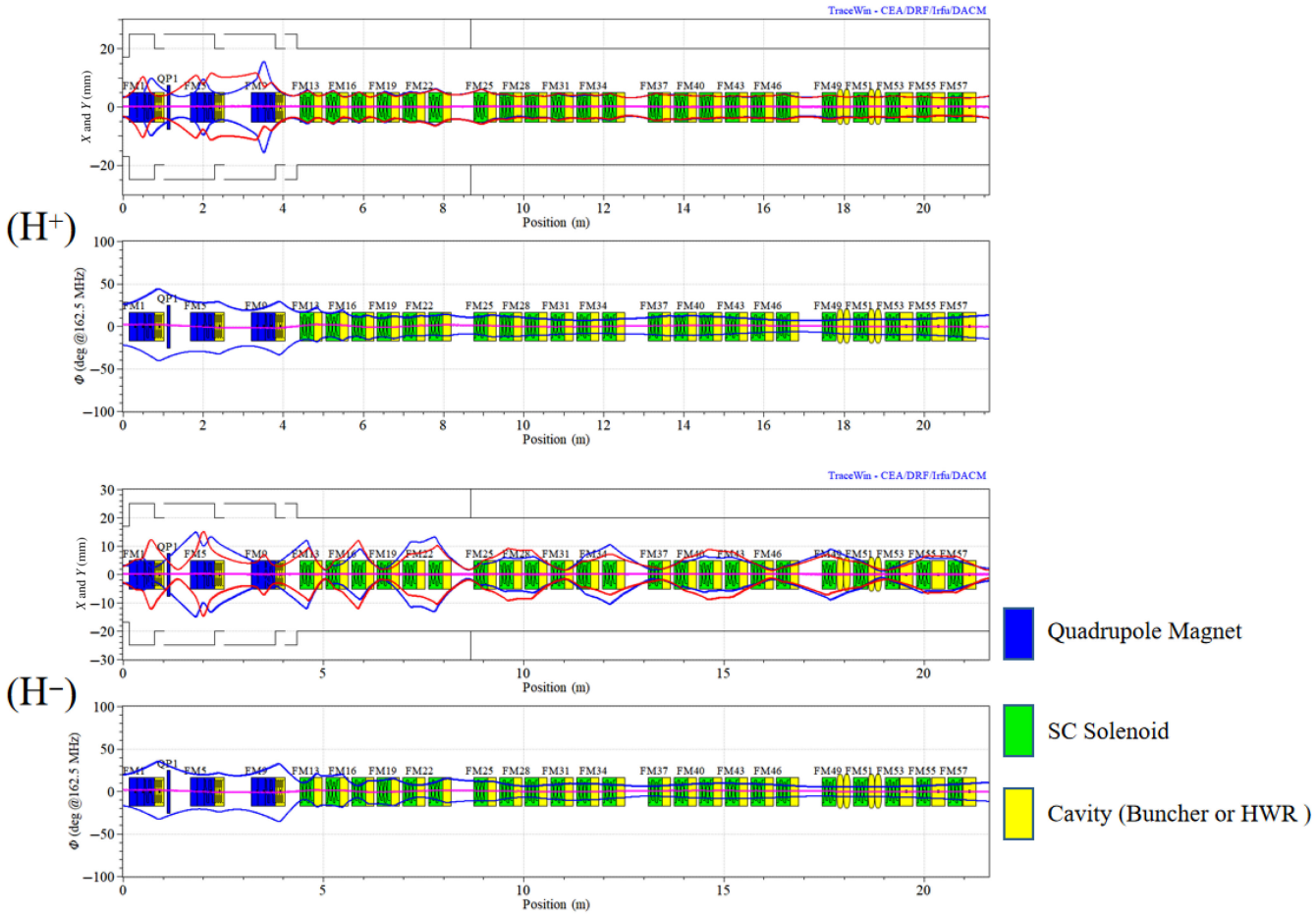


FIG. 6. Multiparticle simulation of proton beam and H^- particles in CAFe (X envelope in blue and Y envelope in red).

gas temperature in K. σ_{cx} denotes the reaction cross section of each reaction channel.

V. QUANTITATIVE ANALYSIS

The cross sections of possible reaction processes and their reaction ratios are shown in Table II [13–17]. It can be seen from the calculation results that the double capture of proton with H_2 is dominant (0.027%) and nearly 2 orders of magnitude more likely than single-electron capture in two processes (0.00038%).

A. Introduction of experimental facility—HIPI

Through extensive literature research and theoretical calculations, we have obtained the theoretical yield of this mechanism. Next, we will conduct measurements of the mechanism's yield based on the high intensity proton implanter (HIPI) [18]. The facility consists of an LEBT, an RFQ, an MEBT, a longitudinal emittance measurement device, and a material irradiation chamber. It can accelerate particles with charge-to-mass ratio of 1/2 up to 1.5 MeV per nucleon. The layout of HIPI is shown in Fig. 7. The beam parameters of the CAFe are shown in Table III.

In this experiment, protons and H^- particles can be separated by using a dipole magnet, by manually changing the polarity of the power supply of the dipole magnet, the beam current of protons and H^- particles can be measured on the Faraday cup located in the MEBT section (MFC2). By incorporating a suppressor electrode into the Faraday cup, the emission of secondary electrons can be effectively suppressed, and interference from external electric fields

TABLE II. Cross sections of possible reaction processes and their reaction ratios.

Reaction	Cross section (cm^2)	Reaction rate (%)
$H^+ + H \rightarrow H^0 + H^+$	8.0×10^{-16}	$\eta_1 = 2.2$
$H^0 + H \rightarrow H^- + H^+$	1.4×10^{-17}	$\eta_2 = 0.038$
$H^+ + H_2 \rightarrow H^0 + H_2^+$	5.2×10^{-16}	$\eta_3 = 1.4$
$H^0 + H_2 \rightarrow H^- + H_2^+$	2.0×10^{-17}	$\eta_4 = 0.054$
$H^+ + H_2 \rightarrow H^- + H^+ + H^+$	1.0×10^{-17}	$\eta_5 = 0.027$
$H^- + H \rightarrow H^0 + H + e$	6.2×10^{-16}	$\eta_6 = 1.7$
$H^- + H_2 \rightarrow H^0 + H_2 + e$	8.0×10^{-16}	$\eta_7 = 2.2$

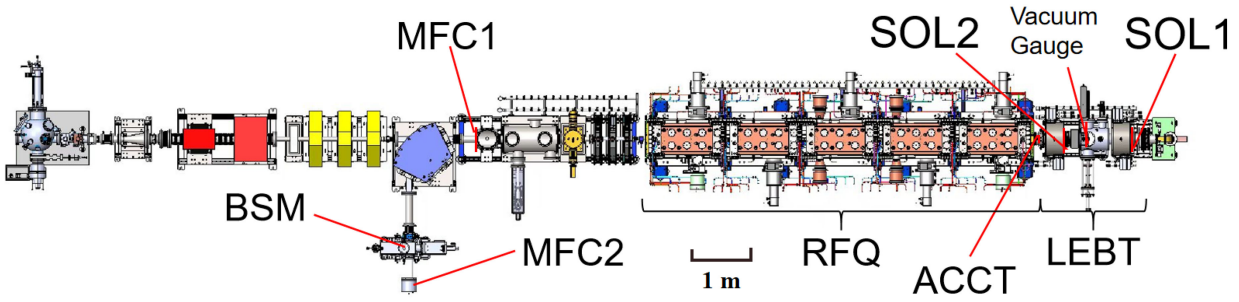


FIG. 7. Layout of HIPI.

can be significantly reduced. This enhancement markedly improves the measurement accuracy of the Faraday cup, achieving a precision of over 95%.

The reasons for conducting this experiment on the HIPI facility require further elaboration. After the beam commissioning of the CAFe accelerator was completed, it was upgraded to CAFe2 for superheavy element research projects. The replaced RFQ accelerator was reused in the HIPI facility. The two facilities also used the same type of ion source and had similar beam parameters. The only difference is that the lengths of LEBT section differ by 0.1 m. On the other hand, compared to the CAFe, the HIPI facility offers a more direct measurement of H^- ions, significantly reducing the errors introduced by the SC section.

B. Measurement experiment of H^- particles

According to Eq. (1), the yield of H^- particles is related to the vacuum pressure, temperature, and length of the LEBT section, as well as the reaction cross section, which is determined by the proton beam energy. Due to the limitations of the actual situation of the accelerator, the mechanical length of the LEBT section and the extraction beam energy from the ion source cannot be changed. This experiment mainly comprises two parts, the measurement of the yield of H^- particles and the measurement of the relationship between the yield and the vacuum pressure. Before the experiment starts, we adjust transmission efficiency of the RFQ to the maximum, thereby improving the signal-to-noise ratio of the readings on MFC2 and making the experimental results more accurate.

TABLE III. Beam parameters of HIPI.

Particle	H^+	
LEBT section energy	20	keV
RFQ output energy	1.5	MeV
Beam current	10	mA
rf frequency	162.5	MHz
Operation mode	cw/pulse	

1. The relationship between the current of the proton beam and H^- particles

Under the condition that the yield of H^- particles remains constant, the beam current of H^- particles should be linearly related to that of the proton beam. To verify this relationship, we conducted the following experiments.

For the ECR proton source used in the HIPI, the beam current of the extracted protons is related to the volume of hydrogen injected, as well as the power and frequency of the microwave power supply. We continuously increased the beam current of the protons extracted from the ion source by increasing the power and frequency of the microwave power supply. Simultaneously, by adjusting the volume of hydrogen injected, we ensured that the pressure of vacuum remained constant during the experiment. The measurement results are shown in Fig. 8. As can be seen from the figure, the current of the H^- particles is directly proportional to that of the proton beam. It can be known from the experimental results that the yield of the H^- particles is 0.08%.

2. The relationship between the yield and the vacuum pressure

Since the yield of H^- particles is closely related to the vacuum pressure, we adjusted the vacuum pressure of the

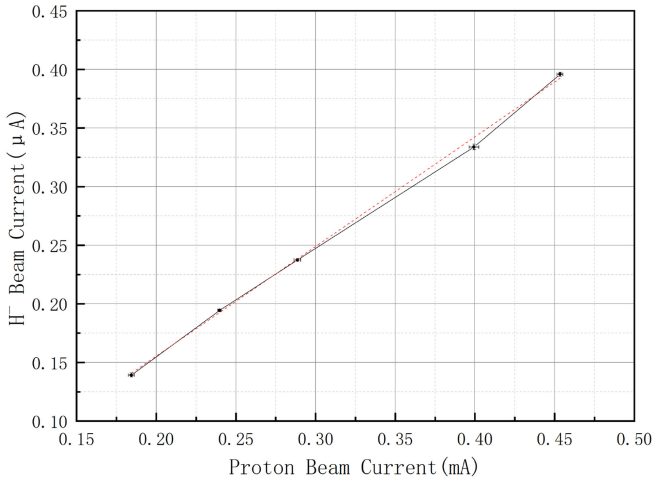


FIG. 8. Relationship between the current of the proton beam and H^- particles.

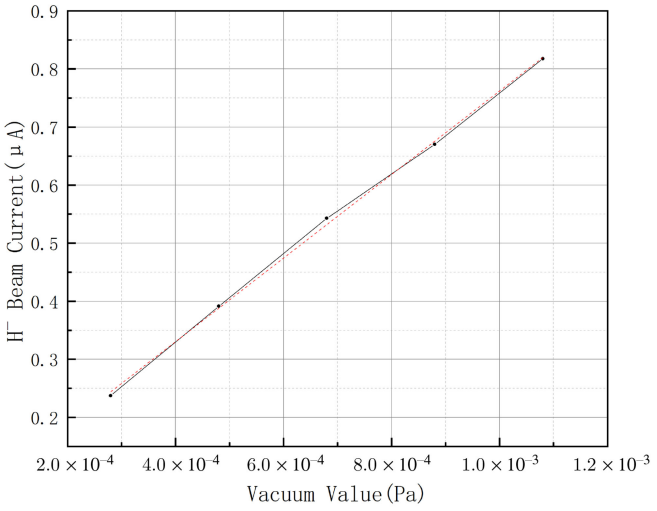


FIG. 9. Relationship between vacuum pressure and the current of H^- particles.

LEBT section by changing the volume of hydrogen injected. To ensure that the beam current of the extracted proton beam remains unchanged, we continuously adjusted the power and frequency of the microwave power supply. Based on the above operations, we measured the relationship between the current of the H^- particles and the vacuum pressure. The measurement results are shown in Fig. 9. The experimental results are consistent with what is described in the Eq. (1). The yield of H^- particles is directly proportional to the vacuum pressure of LEBT section.

VI. DISCUSSION

For HIPI, the length of the LEBT section is 1.53 m. During the experimental process of yield measurement, the vacuum pressure is 2.8×10^{-4} Pa. The theoretical yield of the H^- particles is 0.01%, which is 8 times smaller than the actually measured yield. An analysis was conducted regarding the difference between the theoretical and experimental yields. In the beam vacuum pipe of the LEBT section, as hydrogen gas needs to be continuously injected to maintain the stability of the ion source, the vacuum pressure at the inlet is low, reaching a minimum magnitude of 1×10^{-3} Pa. On the other hand, the outlet of the LEBT is connected to the RFQ, which requires a high vacuum environment in the range of 1×10^{-5} to 1×10^{-6} Pa during operation. However, the HIPI only has one vacuum measuring device located in the middle of the LEBT. The measured vacuum pressure differs significantly from the actual vacuum pressure distribution along the LEBT, and experiments show that the yield of H^- particles is directly proportional to the vacuum pressure. This most likely results in the inconsistency between the experimental and theoretical yield.

In conclusion, for a high-power proton accelerator, unlike other beam loss mechanisms, H^- particles are generated in the LEBT section and are primarily lost in the HEBT section, which will contribute to a high residual radiation dose and cause difficulty for machine maintenance. When the proton beam power is ramped up to MW level, the parasitic H^- particles can reach kW power and may cause machine damage. Several promising schemes to solve the problem are proposed below.

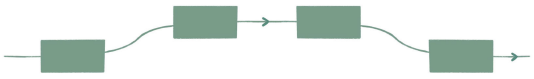


FIG. 10. Sketch map of chicane.

A. Chicane

The H^- particle carries the opposite charge to the proton beam. A chicane is a bump in the beam line made of four bending magnets [19]. The chicane structure shown in Fig. 10 can be used at the exit of the superconducting section, and the H^- particle is deflected in the opposite direction at the first dipole magnet. Using this structure, the filtered H^- particle can be transferred to a terminal via an additional transport line, where it is either dumped or reused. However, for high-power accelerators, the use of multiple dipole magnets may result in an increase in beam losses and may cause machine damage if the beam energy changes or if the chicane dipoles are not tuned correctly.

B. Improvement of LEBT design

According to Eq. (1), the yield of H^- particles in the LEBT section is proportional to the reaction cross section. The yield of H^- particles calculated with Eq. (1) and Table II as a function of energy is shown in Fig. 11. From the figure, the yield of H^- particles reaches its peak at 20 keV, which is the same as the LEBT energy of CAFe. To suppress H^- generation, the energy can be increased to 50 keV or even higher. But this would require a longer RFQ design. Another solution is to improve the vacuum pressure

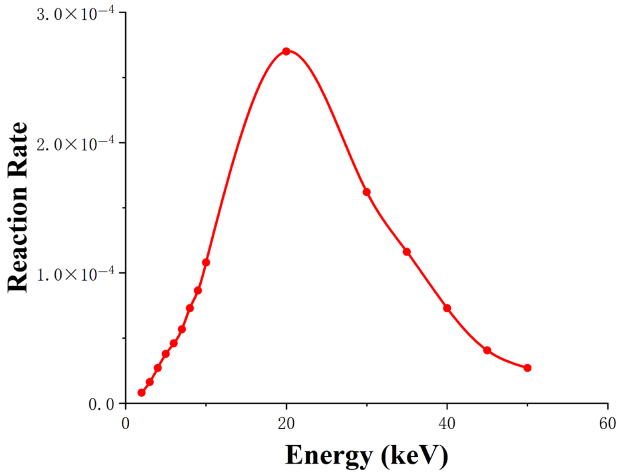


FIG. 11. Variation of the yield of H^- particles with energy.

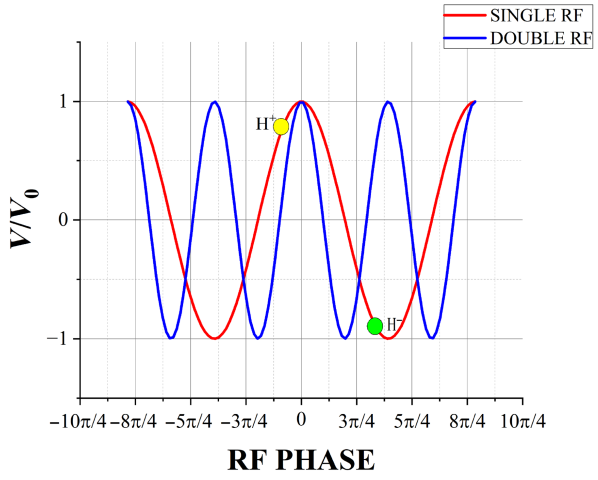


FIG. 12. Schematic of frequency jump.

of the LEBT section. Based on the above experimental results, the yield is proportional to the vacuum pressure in the LEBT section; however, decreasing the vacuum pressure may weaken the effects of space charge neutralization. Thus it is necessary to select an appropriate vacuum pressure to balance these effects [20].

Alternatively, a small-angle dipole magnet can be installed near the end of the LEBT section to separate the H^- particles from the proton beam. The CSNS facility employs this method to remove stripped protons from the H^- beam, and simulation results have demonstrated that a deflection of just 1.8° has negligible impact on the momentum dispersion and emittance growth of the H^- beam [21].

C. Frequency jump in SC section

H^- particles are generated in the LEBT, after RFQ bunching and acceleration, the proton and negative hydrogen beams are centered at their respective synchronous phases, with a phase difference of 180° [22]. As shown in Fig. 12, after doubling the frequency of the SC section, the H^- bunch will enter the section at a phase that is decelerating and longitudinally unstable. Therefore, H^- particles will experience phase slippage and be lost in the SC section [23]. For the CAFe facility, since the rf frequencies of both the RFQ and half-wave resonator (HWR) SC cavities are 162.5 MHz, this effect does not need to be considered. However, for CiADS, multiple frequency jumps occur between different types of cavities [24]. Additional beam loss may occur in the SC section. This needs to be taken into account as the average uncontrolled beam loss should be kept below 1 W/m.

VII. SUMMARY

We discovered a beam loss mechanism in proton accelerators caused by parasitic H^- particles. The yield of this mechanism is mainly related to the length, vacuum pressure, and proton energy of the LEBT section. It needs to be considered in future designs of high-power proton linear accelerators. Appropriate methods need to be adopted in future accelerator design to suppress, eliminate, or utilize parasitic H^- particles.

ACKNOWLEDGMENTS

We would like to express our sincere gratitude to the Large Research Infrastructures China initiative Accelerator Driven System Project (Grant No. 2017-000052-75-01-000590) for their generous support in the completion of this research work. Their financial assistance has been instrumental in enabling us to carry out this research successfully. This research was supported by the National Natural Science Foundation of China (Grants No. 12405189, No. 12475161, No. 11525523, and No. U1730122).

DATA AVAILABILITY

The data that support the findings of this article are openly available [25].

[1] E. Pitcher, R. Sheffield, H. Ait Abderrahim, J. Galambos, Y. Gohar, S. Henderson, G. Lawrence, T. Msanamy, A. Mueller, S. Nagaitsev, J. Nolen, T. Rimmer, and M. Todosow, Accelerator and target technology for accelerator driven transmutation and energy production, DOE White Paper on ADS 1, 10.2172/1847382 (2010).

[2] A. V. Fedotov, Beam halo formation in high-intensity beams, Nucl. Instrum. Methods Phys. Res., Sect. A **557**, 216 (2006).

[3] M. A. Plum, Beam loss in linacs, arXiv:1608.02456.

[4] A. Miura, N. Kikuzawa, T. Maruta, K. Yamamoto, Z. Igarashi, T. Miyao, M. Ikegami, H. Sako, and S. Sato, Status of beam loss evaluation at J-PARC linac, in Proceedings of the 25th International Linear Accelerator Conference (JACoW, Geneva, Switzerland, 2011), TUP076.

[5] A. Miura, M. Ikegami, H. Sako, and G. Wei, Residual gas pressure dependence of beam loss, in *Proceedings of the 25th International Linear Accelerator Conference* (JACoW, Geneva, Switzerland, 2011), TUP075.

[6] R. McCrady, Stripping of H^- beams by residual gas in the linac at the Los Alamos Neutron Science Center, in *Proceedings of the 25th International Linear Accelerator Conference* (JACoW, Geneva, Switzerland, 2011), THP069.

[7] A. Shishlo, J. Galambos, A. Aleksandrov, V. Lebedev, and M. Plum, First observation of intrabeam stripping of negative hydrogen in a superconducting linear accelerator, Phys. Rev. Lett. **108**, 114801 (2012).

[8] S.-H. Liu, Z. Wang, H. Jia, Y. He, W.-P. Dou, Y. Qin, W.-L. Chen, and F. Yan, Physics design of the CIADS 25 MeV demo facility, Nucl. Instrum. Methods Phys. Res., Sect. A **843**, 11 (2016).

[9] M. Khandaker, High purity germanium detector in gamma-ray spectrometry, Int. J. Fundam. Phys. Sci. **1**, 42 (2011).

[10] C. Jin, Z. Wang, X. Qi, Y. He, Z. Li, K. Sun, X. Chen, C. Feng, X. Zhao, Y. Hu, Y. Tian, and K. Li, Advanced virtual accelerator software: A linear accelerator simulation code, Phys. Rev. Accel. Beams **28**, 044602 (2025).

[11] C. Serafim, S. Calatroni, F. Djurabekova, R. Peacock, V. Bjelland, A. Perez Fontenla, W. Wuensch, A. Grudiev, S. Sgobba, A. Lombardi, and E. Sargsyan, Effects of H^- low beam irradiation and high field pulsing tests in different metals, Phys. Rev. Accel. Beams **28**, 013101 (2025).

[12] P. Ewart, *Atomic Physics* (Morgan Claypool Publishers, California, 2019), pp. 2053–2571, 10.1088/2053-2571/aaf801.

[13] A. Jorge, C. Illescas, L. Méndez, and I. Rabadán, Ionization, single and double electron capture in proton-Ar collisions, J. Phys. Chem. A **122**, 2523 (2018).

[14] J. Williams, Single-electron capture and loss cross sections for 2–50-keV hydrogen atoms incident upon hydrogen and the inert gases, Phys. Rev. **153**, 116 (1967).

[15] H. F. Busnengo, S. E. Corchs, and R. D. Rivarola, Single electron capture from molecular hydrogen targets by impact of protons and α particles, Phys. Rev. A **57**, 2701 (1998).

[16] J. Williams, Cross sections for double electron capture by 2–50-keV protons incident upon hydrogen and the inert gases, Phys. Rev. **150**, 7 (1966).

[17] M. W. Gealy and B. Van Zyl, Cross sections for electron capture and loss, Phys. Rev. A **36**, 3091 (1987).

[18] C. Su, Z. Wang, X. Chen, Y. Jia, X. Qi, W. Wang, K. Sun, Y. Du, T. Wang, and Y. Chu, Efficient beam commissioning in HIPI accelerator based on reinforcement learning, Nucl. Instrum. Methods Phys. Res., Sect. A **1072**, 170119 (2025).

[19] J. Tamura, H. Ao, T. Maruta, A. Miura, T. Miyao, and T. Morishita, Development of H^0 beam diagnostic line in MEBT2 of J-PARC linac, in *Proceedings of the 28th Linear Accelerator Conference Linac-2016* (JACoW, Geneva, Switzerland, 2017), 10.18429/JACOW-LINAC2016-MOPLR063.

[20] R. Duperrier, N. Pichoff, D. Uriot, and A. Ismail, Space charge neutralization and its dynamic effects, in *Proceedings of HB2006* (High Energy Accelerator Research Organization, Tsukuba, Ibaraki (Japan), 2006), p. 187.

[21] H. Liao, W. Chen, H. Li, B. Chen, Y. Xiao, Y. Lv, X. Cao, S. Liu, J. Peng, X. Feng, and S. Liu, Removal of stripped protons produced in low-energy beam transport for superconducting linac, Phys. Rev. Accel. Beams **28**, 023502 (2025).

[22] X. QingZi, L. YuZheng, F. ShiNian, and F. ShouXian, Study of simultaneous acceleration of positive and negative ion beams by dynamic simulation in RFQ, High Energy Phys. Nucl. Phys. **28**, 659 (2004).

[23] R. Duperrier, N. Pichoff, and D. Uriot, Frequency jump in an ion linac, Phys. Rev. ST Accel. Beams **10**, 084201 (2007).

[24] Z.-J. Wang, S.-H. Liu, W.-L. Chen, W.-P. Dou, Y.-S. Qin, Y. He, Y.-Z. Jia, C. Feng, M. Yi, Y.-M. Chu, D.-Y. Jia, J.-R. Huang, and H.-W. Zhao, Beam physics design of a superconducting linac, Phys. Rev. Accel. Beams **27**, 010101 (2024).

[25] D. Jia, Data of fig 8&9 of "Investigation of beam loss mechanism by parasitic H^- in high power protonlinac", 10.5281/zenodo.16787828 (2025).